Monitoring of the magnetic field topology and activity of the core helium-burning giant β Ceti in the period 2007 – 2013*

Svetla Tsvetkova[1], Pascal Petit[2,3], Renada Konstantinova-Antova[1], Michel Aurière[2,3], Gregg A. Wade[4], Aline A. Vidotto[5], Corinne Charbonnel[6,2], Ana Borisova[1], Rumen Bogdanovski[1]

[1] Institute of Astronomy and NAO, Bulgarian Academy of Sciences, 72 Tsarigradsko shose, 1784 Sofia, Bulgaria

[2] CNRS, UMR 5277, Institut de Recherche en Astrophysique et Planétologie, 14 Avenue Edouard Belin, 31400 Toulouse, France

[3] Université de Toulouse, UPS-OMP, Institut de Recherche en Astrophysique et Planétologie, Toulouse, France

[4] Department of Physics, Royal Military College of Canada, PO Box 17000, Station 'Forces', Kingston, Ontario, Canada K7K 4B4

[5] School of Physics, Trinity College Dublin, The University of Dublin, Dublin-2, Ireland

[6] Department of Astronomy, University of Geneva, Chemin des Maillettes 51, 1290 Versoix, Switzerland

stsvetkova@astro.bas.bg

(Submitted on 20.07.2018. Accepted on 18.08.2018)

Abstract.

We present a second spectropolarimetric study dedicated to the single giant β Ceti. Adding new data to our previously published data, we are able to trace the evolution of the magnetic activity of the giant for the period from 2007 to 2013. We apply the same data reduction procedures and methods as in our earlier study, so we could reliably compare the results. We reconstruct a third magnetic map, applying the Zeeman Doppler imaging (ZDI) method. From our new observations we recover a dipolar magnetic topology similar to that obtained previously, supporting the long-term stability of the large-scale magnetic field of β Ceti. To visualise the magnetic field lines that extend above the surface, we perform field extrapolations using a potential field method. In contrast to the large-scale field, the behaviour of the activity indicators Hα, Ca II H&K and Ca II IRT suggests an evolution of the small-scale magnetic structures in the chromosphere. This study presents for the first time a long-term monitoring of the magnetic activity of a probable Ap star descendant, which confirms the stability of its large-scale magnetic field.

Key words: cool, giants, magnetic field, magnetic map, long-term stability, β Ceti

1 Introduction

β Ceti (HD 4128) is a slowly rotating single giant ($v \sin i = 3.5$ km s^{-1}) of spectral class K0 III with $V = 2.04$ mag and $B - V = 1.02$ mag. It has the highest X-ray luminosity of $\log L_x = 30.2$ erg/s (Hünsch et al. 1996, Maggio et al. 1998) among the single giants in the near solar neighborhood ($d \leq 30$ pc). It was known that β Ceti is an active giant, because coronal loops (Eriksson et al. 1983) and flares (Ayres et al. 2001) have been reported.

* Based on observations obtained at the Bernard Lyot Télescope (TBL, Pic du Midi, France) of the Midi-Pyrénées Observatory which is operated by the Institut National des Sciences de l'Univers of the Centre National de la Recherche Scientifique of France and Université de Toulouse, and at the Canada-France-Hawaii Telescope (CFHT) which is operated by the National Research Council of Canada, the Institut National des Sciences de l'Univers of the Centre National de la Recherche Scientifique of France, and the University of Hawaii.

Employing modern spectropolarimeters and methods for data reduction, Aurière et al. (2009) measured its photospheric magnetic field for the first time.

The present study is a second paper focusing on the star's magnetic field and its structure. In our previous work (Tsvetkova et al. 2013, hereafter Paper 1), we were able to reconstruct two maps of the surface magnetic field topology of the star for two different epochs (2010 and 2011/2012), employing the Zeeman Doppler imaging (ZDI) technique. Both maps showed that the large-scale magnetic field of β Ceti has a simple topology dominated by the poloidal component. State-of-the-art evolutionary models were also used to show that β Ceti is a 3.5 $M_{\odot}$ giant in the core helium-burning phase with a radius of 18 $R_{\odot}$, and its main sequence progenitor was a late B-type star. Our main conclusion was that the magnetism of β Ceti may well be (at least in part) of fossil origin and inherited from a main sequence Ap/Bp star.

Here, we present new spectropolarimetric observations for the giant β Ceti – one dataset, which contains observations from June to November 2013 with phase coverage sufficient to reconstruct one ZDI map, and some scattered observations in the period from 2007 to 2009. Our aim is to compare the new results with the previous ones, published in Paper 1. In this way, we expect to be able to characterize the evolution of the star's magnetic field over a timespan of almost seven years. In Section 2 we describe the observations and data reduction. In Section 3 we present the new magnetic map of the giant, compute the potential field extrapolations for the three epochs, measure the longitudinal magnetic field B_l, line activity indicators (Hα, Ca II K, Ca II IRT) and radial velocity and examine their variability with time. We end the paper with some conclusions in Section 4.

2 Observations and data reduction

Observations were obtained with two twin fiber-fed échelle spectropolarimeters – Narval (Aurière 2003), which operates at the 2-m Bernard Lyot Telescope (TBL) at Pic du Midi Observatory, France, and ESPaDOnS (Donati et al. 2006a), which operates at the 3.6-m Canada-France-Hawaii Telescope. In polarimetric mode, both instruments have a spectral resolution of about 65 000 and a nearly continuous spectrum coverage from the near-ultraviolet (at about 370 nm) to the near-infrared domain (at 1050 nm) in a single exposure, with 40 orders aligned on the CCD by two cross-disperser prisms. Stokes I (unpolarized light) and Stokes V (circular polarization) parameters are simultaneously obtained by four sub-exposures between which the retarders – Fresnel rhombs – are rotated in order to exchange the beams in the instrument and to reduce spurious polarization signatures (Semel et al. 1993).

The new dataset consists of seven spectra collected in the period June – November 2013. These spectra have a good phase coverage, which is sufficient to reconstruct one ZDI map. Here, we also present some scattered observations from our archive (not published previously) obtained in the period from 2007 to 2009. We add these spectra to the study, because it is essential to use as large a dataset as we can to refine the star's rotation

period. This is described in Section 3.2. The journal of observations is given in Table 1. In the first column of Table 1, the capital letters N and E stand for Narval and ESPaDOnS, respectively. The observations presented in this paper extend over almost 11 rotational cycles of the giant (the value of the rotation period is described in Section 3.2).

We used the same data reduction procedures as for our previous study of β Ceti in Paper 1 – the automatic reduction software LibreEsprit (Donati et al. 1997) and the Least Squares Deconvolution method (LSD, Donati et al. 1997). The LibreEsprit software applies an optimal extraction of the spectrum, wavelength calibration, correction to the heliocentric frame, and continuum normalization to all observations. The LSD method enables averaging of about 12 700 photospheric spectral lines in the case of β Ceti from each spectrum. Thus, the signal-to-noise ratio (S/N) of the LSD Stokes V profile (column 5 in Table 1) is about 30-45 times higher than the S/N of the original spectrum. Mean photospheric Stokes I and V profiles were computed for each spectrum. Then, the longitudinal component of the magnetic field B_l (expressed in gauss) was computed using the first-order moment method (Donati et al. 1997, Rees & Semel 1979, Wade et al. 2000a). More details about the line mask and the LSD method in the case of β Ceti can be found in Paper 1.

Table 1: Journal of observations and measurements of the line activity indicators, the longitudinal magnetic field B_l and radial velocity for the giant β Ceti.

Inst.	Date UT	HJD 2 450 000 +	Rot. phase	S/N (LSD)	S-index	Hα-index	Ca II IRT-index	B_l [G]	σ [G]	RV [km s^{-1}]
(1)	(2)	(3)	(4)	(5)	(6)	(7)	(8)	(9)	(10)	(11)
E	30sep07	4 373.96831	0.000	48 625	0.165	0.279	0.525	3.83	0.54	13.349
E	01oct07	4 374.97454	0.004	46 626	0.169	0.280	0.529	4.22	0.56	13.332
E	02oct07	4 375.97397	0.009	49 079	0.166	0.279	0.523	5.01	0.53	13.353
E	02oct07	4 375.99710	0.009	46 079	0.167	0.280	0.522	4.17	0.57	13.359
E	03oct07	4 376.98558	0.013	52 735	0.167	0.279	0.521	4.45	0.50	13.353
E	03oct07	4 376.98842	0.013	52 735	0.166	0.279	0.522	4.71	0.48	13.352
N	31dec07	4 466.22404	0.404	59 502	0.233	0.274	0.555	6.62	0.44	13.346
N	31dec07	4 466.22947	0.404	59 502	0.226	0.274	0.555	7.37	0.42	13.348
E	22aug08	4 701.05076	1.431	57 885	0.170	0.277	0.526	9.15	0.45	13.379
E	22aug08	4 701.08160	1.431	30 963	0.190	0.277	0.526	8.18	0.85	13.379
E	22aug08	4 701.12813	1.431	36 410	0.183	0.277	0.526	8.63	0.72	13.372
E	22aug08	4 701.13130	1.431	38 227	0.174	0.277	0.527	9.54	0.68	13.371
N	15sep08	4 724.50674	1.533	44 156	0.172	0.275	0.509	4.93	0.55	13.333
N	20sep08	4 729.59068	1.556	43 759	0.167	0.274	0.508	3.11	0.56	13.336
N	24sep08	4 734.47088	1.577	52 278	0.166	0.267	0.507	1.59	0.46	13.365
N	30sep08	4 740.46642	1.603	58 684	0.165	0.268	0.508	0.59	0.45	13.422
E	28sep09	5 102.93453	3.189	77 716	0.165	0.273	0.532	1.13	0.34	13.328
E	02oct09	5 106.94132	3.206	62 306	0.166	0.274	0.529	0.25	0.43	13.295
E	20jun10	5 368.12211	4.349	73 412	0.168	0.278	0.540	4.41	0.36	13.357
E	22jun10	5 370.13397	4.358	63 268	0.168	0.279	0.540	3.89	0.42	13.363

Table 1 Continued:

Inst.	Date UT	HJD 2 450 000 +	Rot. phase	S/N (LSD)	S-index	Hα-index	Ca II IRT-index	B_l [G]	σ [G]	RV [km s^{-1}]
(1)	(2)	(3)	(4)	(5)	(6)	(7)	(8)	(9)	(10)	(11)
E	17jul10	5 395.13970	4.467	78 329	0.195	0.281	0.553	7.36	0.34	13.362
E	18jul10	5 396.13202	4.471	64 598	0.201	0.280	0.553	8.06	0.41	13.378
E	26jul10	5 404.13848	4.506	30 276	0.197	0.281	0.554	8.16	0.88	13.474
E	05aug10	5 414.00630	4.550	64 982	0.196	0.277	0.558	7.17	0.41	13.447
N	07aug10	5 415.63296	4.557	50 740	0.215	0.275	0.535	7.03	0.52	13.439
N	17aug10	5 425.68484	4.601	59 498	0.216	0.279	0.532	4.47	0.46	13.433
N	03sep10	5 442.69880	4.675	55 431	0.212	0.273	0.532	2.75	0.43	13.348
N	19sep10	5 459.47326	4.749	69 382	0.206	0.276	0.529	1.18	0.37	13.359
N	26sep10	5 466.49978	4.779	70 223	0.210	0.276	0.532	0.07	0.37	13.354
N	06oct10	5 475.51782	4.819	40 356	0.223	0.274	0.547	1.81	0.66	13.428
N	13oct10	5 483.47502	4.854	72 465	0.249	0.277	0.560	3.60	0.36	13.439
E	16oct10	5 485.83217	4.864	65 746	0.193	0.276	0.567	3.88	0.41	13.428
E	17oct10	5 486.86076	4.868	68 396	0.216	0.276	0.567	3.58	0.39	13.424
E	17oct10	5 486.86529	4.868	68 396	0.188	0.276	0.565	4.09	0.39	13.424
N	20oct10	5 490.47064	4.884	31 993	0.230	0.277	0.566	5.11	0.82	13.457
N	12nov10	5 513.35989	4.984	37 268	0.214	0.279	0.548	4.90	0.70	13.399
N	26nov10	5 527.36817	5.046	61 161	0.193	0.274	0.535	4.50	0.40	13.257
N	04dec10	5 535.34913	5.080	41 811	0.188	0.278	0.535	4.78	0.58	13.355
N	12dec10	5 543.38259	5.116	29 688	0.185	0.278	0.538	4.96	0.82	13.324
N	14dec10	5 545.29184	5.124	22 465	0.188	0.280	0.545	5.27	1.09	13.234
E	16nov10	5 516.83126	4.999	61 599	0.197	0.282	0.548	3.95	0.43	13.349
E	21nov10	5 521.79751	5.021	59 370	0.185	0.278	0.547	4.19	0.45	13.314
E	22nov10	5 522.71838	5.025	73 414	0.181	0.277	0.545	3.87	0.36	13.336
E	28nov10	5 528.85483	5.052	65 837	0.179	0.277	0.545	3.85	0.40	13.313
E	19jun11	5 732.09718	5.941	29 427	0.192	0.280	0.541	4.29	0.83	13.406
E	22jun11	5 735.12970	5.954	74 032	0.195	0.279	0.539	4.07	0.36	13.415
E	08jul11	5 751.13201	6.024	41 771	0.205	0.279	0.548	4.70	0.64	13.424
E	13jul11	5 756.13434	6.046	52 216	0.214	0.279	0.547	4.18	0.51	13.346
E	15jul11	5 758.13832	6.055	62 607	0.213	0.280	0.551	4.57	0.42	13.393
N	25sep11	5 829.53512	6.367	50 501	0.224	0.275	0.538	6.72	0.52	13.387
N	10oct11	5 845.40689	6.437	47 385	0.218	0.277	0.532	6.02	0.56	13.378
N	30oct11	5 865.44393	6.524	54 215	0.188	0.276	0.524	3.73	0.49	13.383
N	16nov11	5 882.42524	6.599	55 492	0.191	0.279	0.530	4.28	0.44	13.338
N	27nov11	5 893.30869	6.646	60 720	0.199	0.277	0.533	2.71	0.40	13.353
N	08dec11	5 904.31579	6.694	60 838	0.213	0.278	0.545	1.28	0.40	13.349
N	09jan12	5 936.25217	6.834	49 042	0.221	0.278	0.544	3.98	0.50	13.246
N	22jan12	5 949.27910	6.891	61 673	0.198	0.276	0.529	5.23	0.43	13.317
N	30jun13	6 473.62678	9.185	54 401	0.185	0.272	0.532	4.48	0.45	13.316
N	03aug13	6 507.64001	9.334	45 645	0.173	0.273	0.529	7.39	0.57	13.435
N	21aug13	6 525.60524	9.412	63 467	0.197	0.274	0.526	5.76	0.39	13.391
N	04sep13	6 539.57084	9.473	63 890	0.180	0.273	0.528	5.46	0.41	13.359
N	07oct13	6 573.46806	9.622	68 426	0.180	0.275	0.513	0.68	0.39	13.366
N	07nov13	6 604.38624	9.757	48 223	0.193	0.275	0.526	0.54	0.55	13.425
N	27nov13	6 624.31154	9.844	39 420	0.197	0.278	0.534	3.51	0.63	13.260

3 Results

3.1 Measurements of the averaged longitudinal magnetic field, line activity indicators and radial velocity

All the measurements of the averaged longitudinal magnetic field and its error bars, line activity indicators and radial velocity are presented in Table 1 and Fig. 1. The years of observations are labeled at the top of the figure.

The longitudinal magnetic field B_l was inferred by measuring the first order moment of the Stokes V LSD profiles (Rees & Semel 1979, Donati et al. 1997, Wade et al. 2000a). Since we employ the same procedure and parameters to process the observations, we refer the reader to Paper 1 for more details.

In spite of having only 7 spectra for the 2013 dataset, it is obvious from Fig. 1 (top panel) that B_l follows the same trend of time variability as for the previous two datasets from 2010 and 2011/2012 – it still remains of positive polarity and shows sinusoidal-like variations with time. Such variations of the longitudinal magnetic field B_l are typical for Ap stars (Aurière et al. 2007, Wade et al. 2000a, b, Kochukhov & Wade 2010, Silvester et al. 2012), and are characteristic of a globally-organized dipole field configuration (Landstreet & Mathys 2000). The observations from 2007 to 2009 are not sufficient to show the detailed variability of B_l during that period; still, they show that there is no change in its sign and amplitude.

The radial velocity (RV) is a photospheric characteristic like B_l, which is usually also affected by the rotational modulation. We measured the RV of the LSD Stokes I line profiles by performing χ^2 adjustment of a Gaussian function on the line core and then taking the central velocity of the Gaussian as our RV value. We use the same procedure here as in Paper 1. The radial velocity stability of ESPaDOnS and Narval is about 0.03 $\mathrm{km\,s^{-1}}$ (Moutou et al. 2007, Donati et al. 2008). The goodness of the Gaussian fit is about 0.01 $\mathrm{km\,s^{-1}}$. In the case of β Ceti, the time variability of RV is rather similar for the three datasets presented in Fig. 1, especially for the first and third datasets. This indicates that β Ceti shows a very stable large-scale magnetic field configuration for the observational interval from 2010 to 2013. The scattered observations from 2007 to 2009 do not differ significantly from later observations.

The observed additional heating in the chromosphere of magnetically active stars is caused by magnetohydrodynamic waves, Ohmic dissipation and magnetic field reconnections (Linsky 1980, 1985). Because of that extra heating, there is a radiative excess in spectral lines, mainly those from singly ionized metals and neutral hydrogen (Wilson 1968, Skumanich et al. 1975, Anderson & Athay 1989, Narain & Ulmschneider 1990, 1996). This is the reason the core emission of the Ca II H&K line and the absorption lines Hα and Ca II infrared triplet (IRT) – partially filled-in by emission – are widely used as classical line activity indicators.

In Paper 1 we measured the depths of these three lines. In order to achieve a better precision of the measurements in this paper, we computed

the indices of the lines instead. We used the method presented by Marsden et al. (2014) for the Hα and Ca II IRT indices. For the S-index we also followed the method given by Marsden et al. (2014), but with calibration coefficients adjusted for cool giants (Aurière et al. 2015). The values of these coefficients for Narval and ESPaDOnS are summarized by Tsvetkova et al. (2017). Thus, the three line indices of β Ceti for all the spectra from 2007 to 2013 were measured and the results are presented in Table 1 and Fig. 1. The precision of each measurement is between 0.003 to 0.009.

Relations between indices of each pair of these three lines have been analyzed using the linear Pearson correlation coefficient r. The three plots are shown in Fig. 2 and the values of the corresponding Pearson coefficients are given in the upper left corner of each plot. Each year of observations is identified by a different color and symbol. A relatively good correlation is achieved between the Ca II IRT-index and S-index. There is no correlation between the Hα-index and the S-index.

The behaviour of the Hα and S-indices have been studied for several samples of FGKM main sequence stars (Cincunegui et al. 2007, Gomes da Silva et al. 2011, 2014) and the Pearson coefficients vary from -1 to 1. The authors of those studies concluded that low values of the coefficients should be a result of the low activity levels of the stars. An important fact is that the emission cores of the Hα and Ca II H&K lines are formed at different optical depths in the stellar chromosphere (which is highly extended for a late-type giant as β Ceti). The different contributions of activity-related features (such as filaments and plages) and their different spatial distributions on the stellar disk can also decrease the correlation between the two indices (Meunier & Delfosse 2009, Gomes da Silva et al. 2011). Meunier & Delfosse (2009) and Gomes da Silva et al. (2014) showed that the correlation can also be underestimated if the observations do not cover a full activity cycle. This idea is very well confirmed by two cool main sequence active stars – ξ Bootis A (Morgenthaler et al. 2012) and HN Peg (Boro Saikia et al. 2015). The long-term monitoring of these two stars highlighted a correlation between chromospheric emission in various spectral lines, but the correlation is only visible while grouping together data at various phases of the long-term magnetic cycle (hence with very different emission values), while the correlation was much weaker (and sometimes absent) for individual epochs.

Thus, the low values of the Pearson coefficients of β Ceti could be due to an evolution of the small-scale magnetic features in the chromosphere during different observational epochs, which is also noticeable from the decrease in 2013 of the averaged values of the three lines compared to 2010 and 2011/2012 observations (Fig. 1), in addition to the fact that our observational data do not cover a full activity cycle of the giant.

3.2 The rotation period of β Ceti

We searched for a rotation period of β Ceti in Paper 1, using the spectropolarimetric data we had collected at that time, i.e. spectra from 2010 to 2012. We followed the approach of Petit et al. (2002), which basically consists of the following steps. First, we computed two hundred ZDI models, assuming a different value for the rotation period for each model. The

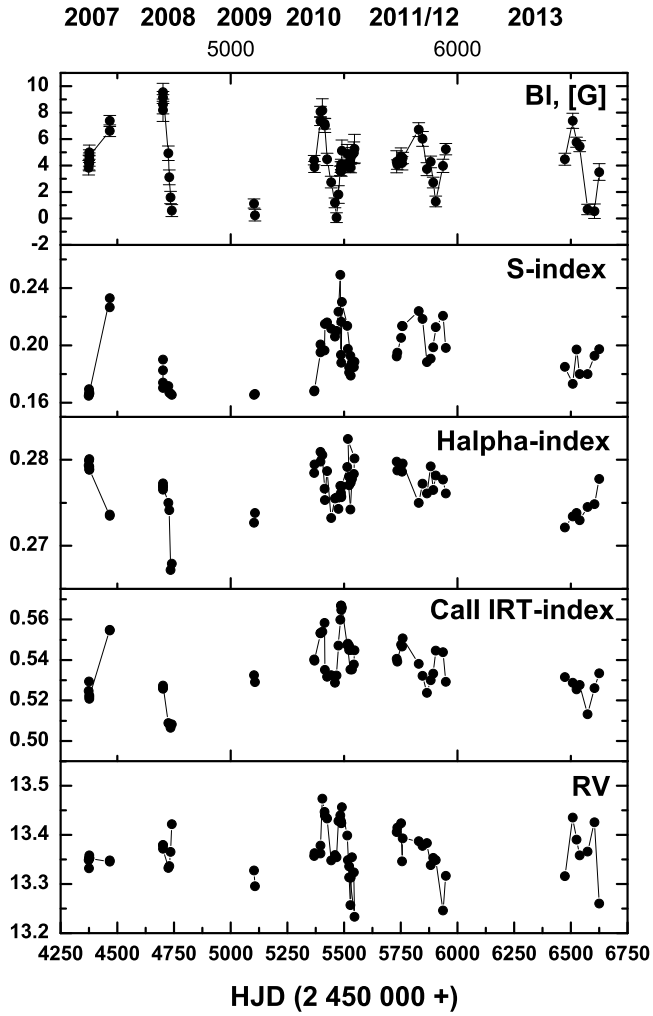

Fig. 1. From top to bottom are presented the variations in B_l, S-index, Hα-index, Ca II IRT-index, and the radial velocity from 2007 to 2013. The B_l and RV data from 2010 and 2011/2012 were published in Paper 1.

interval we searched in was between 100 and 300 days. All models had the same averaged magnetic field strength. Then, the models were compared to the observed Stokes V profiles. The best magnetic model was identified by the lowest χ^2 value. Applying this approach in Paper 1, we determined a rotation period of 215 days for β Ceti.

Our new dataset from 2013 consists of only 7 spectra, which do not cover completely one rotational cycle of the giant. Running a periodogram

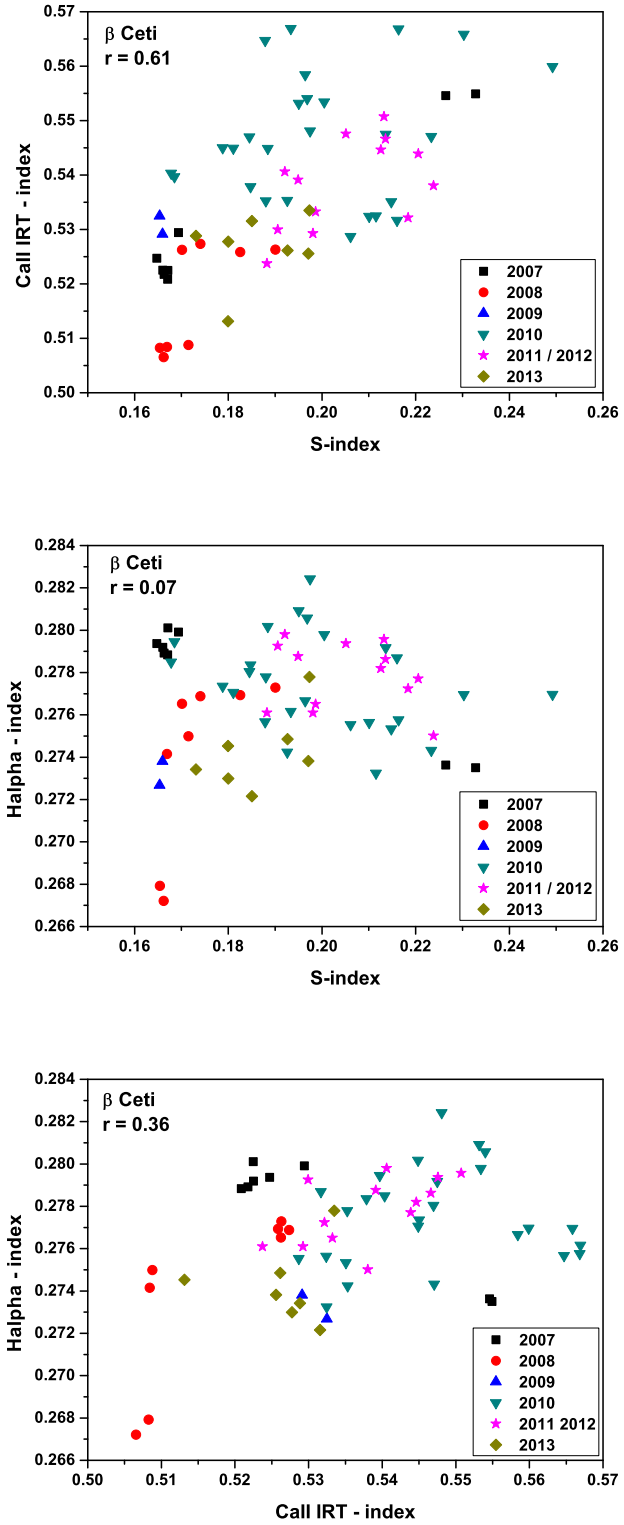

Fig. 2. Line-line relations – from top to bottom: Ca II IRT-index vs. S-index; Hα-index vs. S-index; Hα-index vs. Ca II IRT-index. Each year of observations is identified by a different color and symbol. The corresponding value of the Pearson coefficient is given in the upper left corner of each plot.

analysis over this short dataset itself would not give any reasonable value for a period. Instead, we again applied our approach for a period search, using the spectra for all seven years. We computed 300 models and searched in the interval between 100 and 300 days. We present the resultant periodogram in Fig. 3. The lowest χ^2 value suggests a period of 228.6 days. Thus, using a longer timespan than in Paper 1, we are able to achieve a better determination of the period. The refining of the value is very well demonstrated in Fig. 4, where variations of B_l are phased with the new value of the period, according to the following ephemeris:

$$HJD = 2454373.9 + 228.6\,\phi \quad (1)$$

where HJD is the heliocentric Julian date of the observations and ϕ is the rotational phase, which is given in the fourth column of Table 1. The HJD_0 is chosen to match the first spectrum of β Ceti (September 30, 2007).

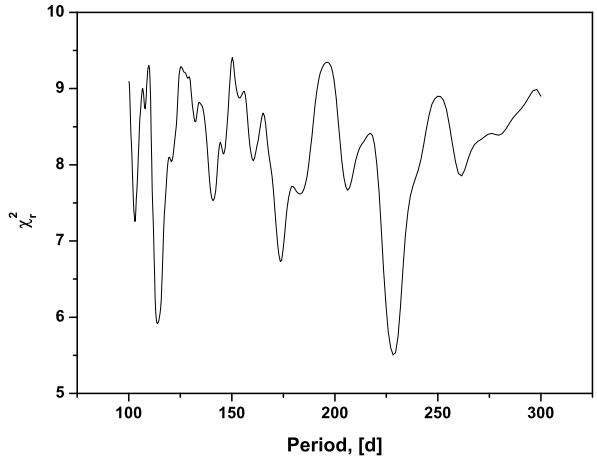

Fig. 3. Periodogram obtained with all the spectra from 2007 to 2013.

Easily distinguished sinusoidal variations of B_l with time first shown in Fig. 1 are repeated in Fig. 4, in which the data are phased with a period of 228.6 days, which is a good confirmation that this value of the period is accurate.

3.3 Zeeman Doppler Imaging

To map the stellar surface magnetic field from sets of rotationally modulated circularly polarized profiles of spectral lines, we used the Zeeman Doppler Imaging tomographic method (ZDI, Semel 1989, Donati & Brown 1997, Donati et al. 2006b). Since we employed the same ZDI method in

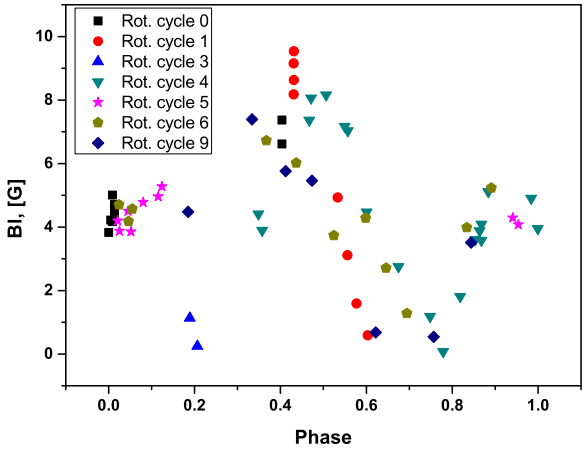

Fig. 4. Variations of B_l (from 2007 to 2013) with phase, assuming a rotation period of 228.6 days. Each rotational cycle is identified by a different color and symbol according to the legend of the plot.

this paper as in Paper 1, details about the application of this procedure to β Ceti can be found there. Except for the rotation period, which we discussed in the previous section, the other input parameters for the current ZDI model are the same as we used in Paper 1: limb darkening coefficient set to 0.75 (Claret & Bloemen 2011); spherical harmonics expansion set to $l \leq 10$; $v \sin i = 3.5$ km s^{-1}; inclination angle $i = 60°$. All data are phased according to equation (1).

The signal-to-noise ratio (S/N) of each Stokes V LSD profile is given in the fifth column in Table 1. The Stokes V profiles for each of the three observational epochs (2010, 2011/2012, 2013) are shown in Fig. 5. All the profiles from the three panels show simple shapes with positive blue lobes and negative red lobes, which is consistent with the measured positive values of B_l.

The three magnetic maps of β Ceti reconstructed with the new value of the rotation period are shown in Fig. 6. These maps correspond to magnetic models with $\chi^2_r = 2.2$ for 2010, $\chi^2_r = 2.0$ for 2011/2012 and $\chi^2_r = 1.3$ for 2013. In general, the dipolar structure is clearly visible in the three radial maps. Similar magnetic structures are reconstructed around phase 0.8. On the other hand, it seems that there is a change of the magnetic structure around phase 0.2. Actually, it is hard to say whether this is a real evolution, because in 2013 there is only one observation between phases 0.0 and almost 0.3, while in 2010 and 2011/2012 there are no observations between 0.1 and 0.3. A real but small change can be noticed between the two radial maps of 2010 and 2011/2012 in the phase interval 0.0 - 0.1. Another apparently real change is the bump with positive polarity, which moves slightly around phase 0.4 in the three maps.

Despite these suspected evolutions of the photospheric magnetic structures on relatively small spatial scales, for all the three epochs the large-scale magnetic geometry is dominated by the poloidal component of the magnetic field, which contains about 98% of the reconstructed magnetic energy. Most of the magnetic energy of the poloidal component is stored in spherical harmonic modes with $l = 1$ (dipole), which contain more than 84% of the reconstructed poloidal energy (Table 2).

Table 2. Magnetic characteristics of β Ceti for the three epochs.

Epoch	B_{max} [G]	pol. comp. (% tot)	dipole comp. (% pol)	quad. comp. (% pol)	oct. comp. (% pol)	axi. comp. (% tot)
2010	19	98	87	8	4	87
2011/2012	19	98	87	3	2	84
2013	14	98	84	6	7	79

Note: Third column – the fraction of the large-scale magnetic energy reconstructed in the poloidal field component; forth to sixth columns – list the fraction of the poloidal magnetic energy stored in the dipolar ($l = 1$), quadrupolar ($l = 2$) and octopolar ($l = 3$) components; seventh column – the fraction of the large-scale magnetic energy stored in the axisymmetric component ($m = 0$).

3.4 Extrapolation of the magnetic field

To visualise the three-dimensional magnetic field of β Ceti extrapolated into its chromospheric region, we use the potential field source surface (PFSS) extrapolation (Altschuler & Newkirk 1969, Jardine et al. 2002, Vidotto et al. 2013). This method, originally developed to study the solar coronal magnetic field and extended to low-mass main sequence stars, assumes that the field is potential field ($\nabla \times \boldsymbol{B} = 0$), i.e., there are no currents. The extrapolation is done from the surface of the star out to the radius of the source surface, which is chosen. At the surface of the star, the radial magnetic field is set to the observed value (presented in Fig. 5), while the azimuthal and meridional components are calculated as to obey the potential assumption. The outer boundary, known as the source surface, is the distance, beyond which, the magnetic field lines are purely radial. This has the effect of emulating the radial stretching of magnetic field lines, believed to be caused by stellar winds. In the Sun, the source surface is around 2 - 4 solar radii. These values are derived, for example, from solar eclipse images. In the case of β Ceti, we do not have observations to constrain the distance to the source surface. Thus, we adopt a value of 3.4 R_{star}, similar to the solar value. Our extrapolations for the three epochs are shown in Fig. 7, where we clearly visualise the large-scale dipolar structure of β Ceti.

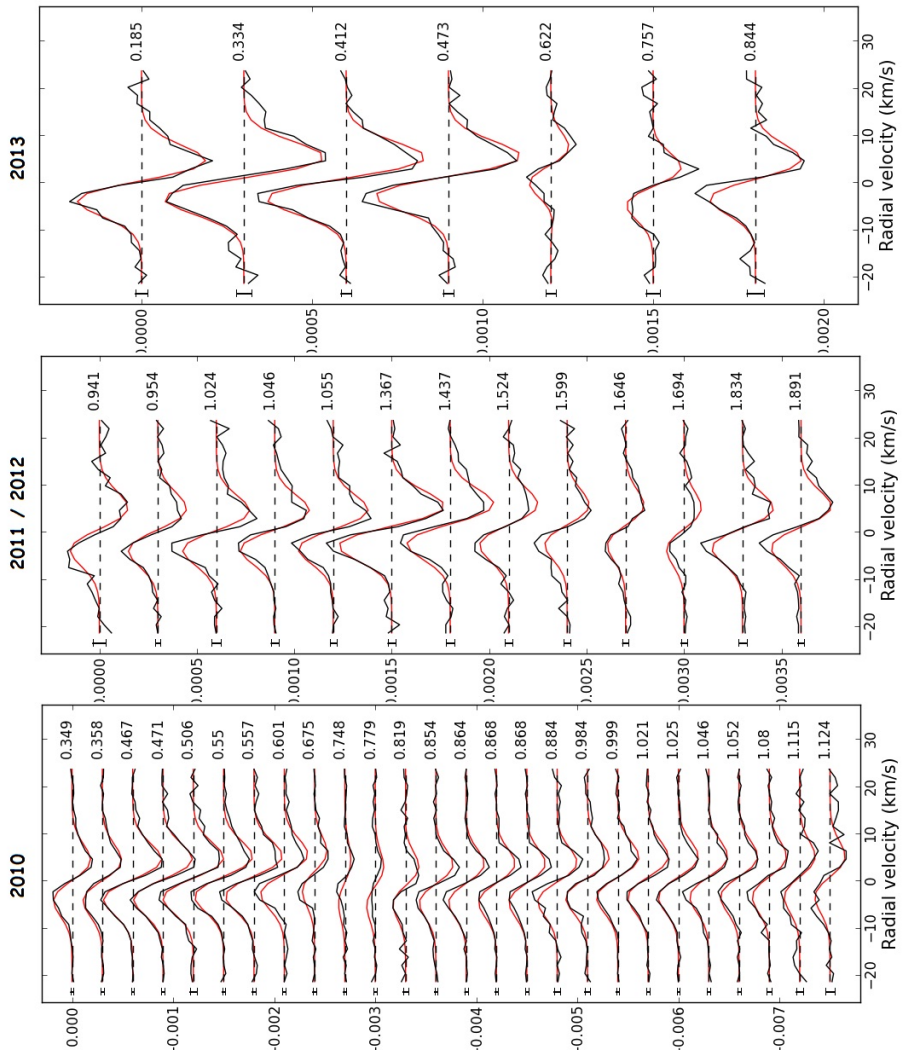

Fig. 5. Normalized Stokes V profiles of β Ceti – observed profiles (black lines); synthetic profiles (red lines); zero level (dashed lines). All profiles are shifted vertically for display purposes. The rotational phases of observations are indicated in the right part of the plot and the error bars are on the left of each profile. The epoch of observations is indicated on top of each plot.

4 Conclusion

This study is an extension of our work in Paper 1. Here, we present new spectropolarimetric observations, obtained with the same equipment and processed with the same methods as in Paper 1. The long-term observational interval enables us to analyse the magnetic field of the giant β Ceti for almost 10 rotational cycles.

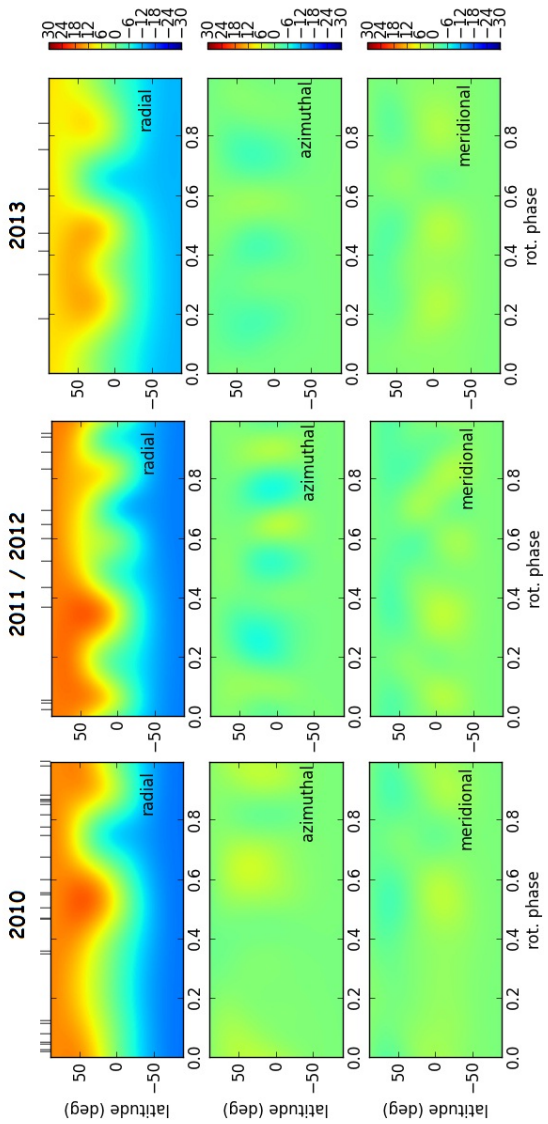

Fig. 6. Magnetic maps of β Ceti for the three epochs of observations. Each panel has three maps, which illustrate the field components in spherical coordinates (from top to bottom – radial, azimuthal, meridional). The magnetic field strength is expressed in gauss. The vertical ticks on top of the radial maps show the phases of observations.

The behaviour of the chromospheric line activity indicators and the line-line correlations (shown in Fig. 1 and Fig. 2) show that the small-scale magnetic structures in the chromosphere of β Ceti change slightly with time, which could be expected for a convective giant with an extended

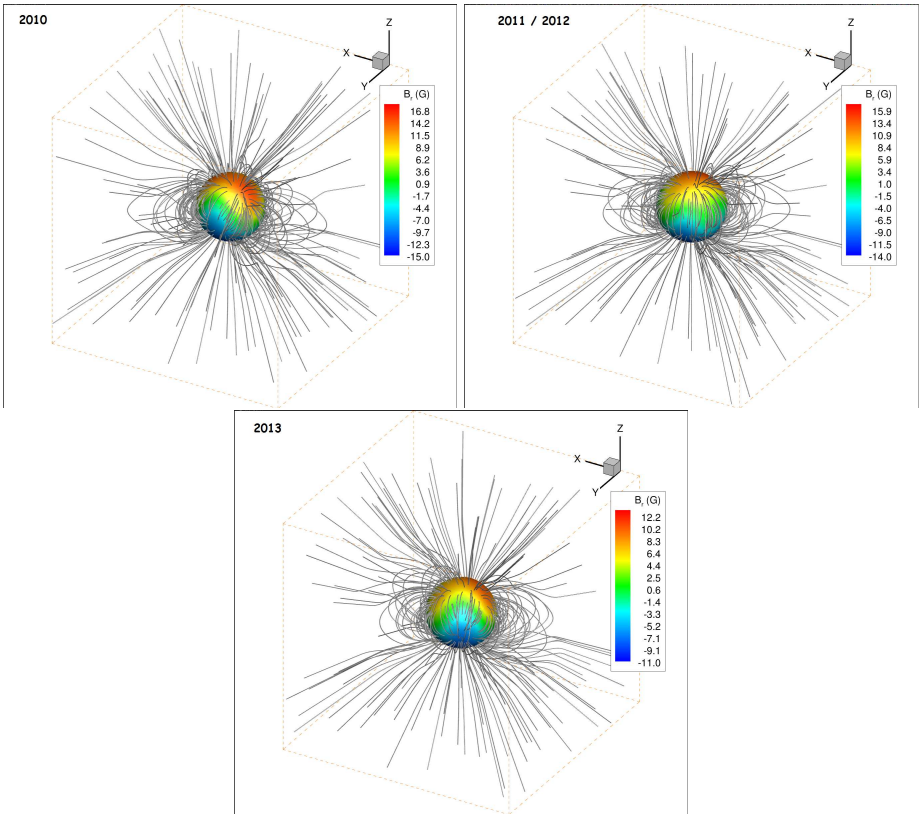

Fig. 7. The three-dimensional configuration of the magnetic field of β Ceti, extrapolated from its surface (values from ZDI maps) into its chromospheric region. The epoch is shown on the top left corner of each panel.

atmosphere – β Ceti has a radius of 18 $R_\odot$ and it is in the core helium-burning phase (Paper 1). The three radial ZDI maps from Fig. 6 also can give a hint about a variability of the photospheric magnetic field presented just by some localised features of the polar spot, which could be a result of the interaction between the magnetic field and convection. But globally, β Ceti shows a stable poloidal component for the interval from 2010 to 2013 (6 rotational cycles) – this component contains about 98% of the magnetic energy for each map. The dipole structure dominates over the three ZDI maps, with more than 84% of the poloidal energy. The dipole structure is also clearly visible in the 3D field extrapolations (Fig. 7). The scattered observations between 2007 and 2009 also do not suggest a different behaviour of the photospheric (B_l and RV) and chromospheric (Hα, Ca II H&K, Ca II IRT) magnetic proxies (Fig. 1), compared to the period from 2010 to 2013.

Compared to two other studied giants that are suspected as Ap star descendants, EK Eri (Aurière et al. 2011) and OU And (Borisova et al.

2016), β Ceti is the most evolved Ap star descendant known up to now. The present study revealed that being in helium burning phase, β Ceti still keeps a stable global dipolar structure (typical for Ap stars; Wade et al. 2000c, Silvester et al. 2012, 2014), nevertheless the long time convection takes place in its interior.

Acknowledgements

We thank the TBL and CFHT teams for providing service observing with Narval and ESPaDOnS. The observations in 2010 with Narval were funded under Bulgarian NSF grant DSAB 02/3/2010. The observations in 2013 with Narval were funded under the contract BG051PO001-3.3.06-0047. S.Ts. acknowledges the financial support from the contract DFNP-104 under the program for career development of young scientists, BAS. R.K.-A., S.Ts. and A.B. thank the project DN 08-1/2016 funded under the Bulgarian Ministry of Education and Science by National Science Fund of Bulgaria. G.A.W. acknowledges support from the Natural Sciences and Engineering Research Council of Canada (NSERC).

References

Altschuler, M.D. & Newkirk, G. 1969, SoPh, 9, 131
Anderson, L.S. & Athay, R.G. 1989, ApJ, 346, 1010
Aurière, M. 2003, in "Magnetism and Activity of the Sun and Stars", Eds J. Arnaud and N. Meunier, EAS Publ. Series 9, 105
Aurière, M., Wade, G.A., Silvester, J. et al. 2007, A&A, 475, 1053
Aurière, M., Konstantinova-Antova, R., Petit, P., Wade, G. & Roudier, T. 2009, IAUS, 259, 431
Aurière, M., Konstantinova-Antova, R., Petit, P. et al. 2011, A&A, 534, 139
Aurière, M., Konstantinova-Antova, R., Charbonnel, C. et al. 2015, A&A, 574, 90
Ayres, T.R., Osten, R.A. & Brown, A. 2001, ApJ, 562, L83
Borisova, A., Aurière, M., Petit, P. et al. 2016, A&A, 591, 57
Boro Saikia, S., Jeffers, S.V., Petit, P. et al. 2015, A&A, 573, 17
Cincunegui, C, Díaz, R.F. & Mauas, P.J.D. 2007, A&A, 469, 309
Claret, A. & Bloemen, S. 2011, A&A, 529, 75
Donati, J.-F. & Brown, S.F. 1997, A&A, 326, 1135
Donati, J.-F., Semel, M., Carter, B.D., Rees, D.E. & Collier Cameron, A. 1997, MNRAS, 291, 658
Donati, J.-F., Catala C., Landstreet J. & Petit P. 2006a, in Casini R., Lites B., eds, Solar Polarization Workshop n4 Vol.358 of ASPC series, 362
Donati, J.-F., Howarth, I.D., Jardine, M.M. et al. 2006b, MNRAS, 370, 629
Donati, J.-F., Morin, J., Petit, P. et al. 2008, MNRAS, 390, 545
Eriksson, K., Linsky, J.L. & Simon, T. 1983, ApJ, 272, 665
Gomes da Silva, J., Santos, N.C., Bonfils, X. et al. 2011, A&A, 534, 30
Gomes da Silva, J., Santos, N.C., Boisse, I. et al. 2014, A&A, 566, 66
Hünsch, M., Schmitt, J.H.M.M., Schröder, K.-P. & Reimers, D. 1996, A&A, 310, 801
Jardine, M., Collier Cameron, A., Donati, J.-F. 2002, MNRAS, 333, 339
Kochukhov, O. & Wade, G.A. 2010, A&A, 513, 13
Landstreet, J.D. & Mathys, G. 2000, A&A, 359, 213
Linsky, J.L. 1980, ARA&A, 18, 439
Linsky, J.L. 1985, in: Progress in stellar line formation theory, Beckman J.E. & Coivelory L. (eds), 1
Maggio, A., Favata, F., Peres, G. & Sciortino, S. 1998, A&A, 330, 139
Marsden, S.C., Petit, P., Jeffers, S.V. et al. 2014, MNRAS, 444, 3517
Meunier, N. & Delfosse, X. 2009, A&A, 501, 1103
Morgenthaler, A., Petit, P., Saar, S. et al. 2012, A&A, 540, 138

Moutou, C., Donati, J.-F., Savalle, R. et al. 2007, A&A, 473, 651
Narain, U. & Ulmschneider, P. 1990, SSRv, 54, 377
Narain, U. & Ulmschneider, P. 1996, SSRv, 75, 453
Petit, P., Donati, J.-F. & Collier Cameron, A. 2002, MNRAS, 334, 374
Rees, D.E. & Semel, M.D. 1979, A&A, 74, 1
Semel, M. 1989, A&A, 225, 456
Semel, M., Donati, J.-F. & Rees, D.E. 1993, A&A, 278, 231
Silvester, J., Wade, G.A., Kochukhov, O. et al. 2012, MNRAS, 426, 1003
Silvester, J., Kochukhov, O. & Wade, G.A. 2014, MNRAS, 440, 182
Skumanich, A., Smythe, C. & Frazier, E.N. 1975, ApJ, 200, 747
Tsvetkova, S., Petit, P., Aurière, M. et al. 2013, A&A, 556, 43 (Paper 1)
Tsvetkova, S., Petit, P., Konstantinova-Antova, R. et al. 2017, A&A, 599, 72
Vidotto, A.A., Jardine, M., Morin, J. et al. 2013, A&A, 557, 67
Wade, G.A., Donati, J.-F., Landstreet, J.D. & Shorlin, S.L.S. 2000a, MNRAS, 313, 823
Wade, G.A., Donati, J.-F., Landstreet, J.D. & Shorlin, S.L.S. 2000b, MNRAS, 313, 851
Wade, G.A., Debernardi, Y., Mathys, G. et al. 2000c, A&A, 361, 991
Wilson, O. C. 1968, ApJ, 153, 221